MNRAS **461,** 1927–1936 (2016)
Advance Access publication 2016 June 20
doi:10.1093/mnras/stw1449

The detection and X-ray view of the changing look AGN HE 1136-2304

M. L. Parker,[1★] S. Komossa,[2] W. Kollatschny,[3] D. J. Walton,[4,5] N. Schartel,[6] M. Santos-Lleó,[6] F. A. Harrison,[5] A. C. Fabian,[1] M. Zetzl,[3] D. Grupe,[7] P. M. Rodríguez-Pascual[6] and R. V. Vasudevan[1]

[1]*Institute of Astronomy, Madingley Road, Cambridge CB3 0HA, UK*
[2]*Max-Planck-Institut für Radioastronomie, Auf dem Hügel 69, D-53121 Bonn, Germany*
[3]*Institut für Astrophysik, Universität Göttingen, Friedrich-Hund-Platz 1, D-37077 Göttingen, Germany*
[4]*Jet Propulsion Laboratory, California Institute of Technology, 4800 Oak Grove Drive, Pasadena, CA 91109, USA*
[5]*California Institute of Technology, 1200 East California Boulevard, Pasadena, CA 91125, USA*
[6]*XMM–Newton SOC, ESA, ESAC, Villafranca del Castillo, Camino Bajo del Castillo s/n, E-28692 Villanueva de la Cañada Madrid, Spain*
[7]*Department of Earth and Space Science, Morehead State University, 235 Martindale Drive, Morehead, KY 40351, USA*

Accepted 2016 June 15. Received 2016 June 15; in original form 2016 March 5

ABSTRACT

We report the detection of high-amplitude X-ray flaring of the AGN HE 1136-2304, which is accompanied by a strong increase in the flux of the broad Balmer lines, changing its Seyfert type from almost type 2 in 1993 down to 1.5 in 2014. HE 1136-2304 was detected by the *XMM–Newton* slew survey at >10 times the flux it had in the *ROSAT* all-sky survey, and confirmed with *Swift* follow-up after increasing in X-ray flux by a factor of ∼30. Optical spectroscopy with SALT shows that the AGN has changed from a Seyfert 1.95 to a Seyfert 1.5 galaxy, with greatly increased broad line emission and an increase in blue continuum AGN flux by a factor of >4. The X-ray spectra from *XMM–Newton* and *NuSTAR* reveal moderate intrinsic absorption and a high energy cutoff at ∼100 keV. We consider several different physical scenarios for a flare, such as changes in obscuring material, tidal disruption events, and an increase in the accretion rate. We find that the most likely cause of the increased flux is an increase in the accretion rate, although it could also be due to a change in obscuration.

Key words: accretion, accretion discs – black hole physics – galaxies: active – galaxies: Seyfert.

1 INTRODUCTION

Outbursts in radio-quiet active galactic nuclei (AGN) are a relatively unexplored area of AGN physics. However, observations of these unusual events have the potential to trace accretion physics in detail, particularly when multiple instruments can be used to observe at different wavelengths. In recent years, there have been several detections of AGN in anomalously low or high X-ray states using *Swift* monitoring or *XMM–Newton* surveys (e.g. Schartel et al. 2007, 2010; Miniutti et al. 2009, 2013; Grupe et al. 2012, 2013; Gallo et al. 2015; Parker et al. 2014a,b; Saxton et al. 2014; Grupe, Komossa & Saxton 2015; Komossa et al. 2015). Despite the high-amplitude X-ray variability (factors > 20–100) of AGN, these events rarely come with strong changes in the optical emission lines, implying that the observed changes mostly happen along our line of sight, and do not affect the bulk of the emission-line regions. An interesting example is GSN 069, which was detected during an *XMM–Newton* slew observation in 2010 at a soft X-ray flux level at least 240 times that which it had when *ROSAT* failed to detect it in 1994 (Miniutti et al. 2013). The X-ray spectrum is extremely soft and unobscured, and it shows rapid soft X-ray variability, which is consistent with Seyfert 1 behaviour. However, it has no detected broad line emission, so can be classified as a Seyfert 2.

The term 'changing look' was coined to refer to X-ray observations of Compton-thick AGN becoming Compton-thin, and vice-versa (Guainazzi 2002; Guainazzi et al. 2002; Matt, Guainazzi & Maiolino 2003; Marchese et al. 2012; Miniutti et al. 2014; Ricci et al. 2016). This transition can be extremely rapid: Risaliti et al. (2005) found NGC 1365 switching from Compton thick to Compton thin in under 6 weeks. There are also well documented cases of changing-look behaviour in the optical band, where the optical spectra of AGN change so as to move to a different Seyfert classification. Cases include NGC 3515 (Collin-Souffrin, Alloin & Andrillat 1973), NGC 7306 (Tohline & Osterbrock 1976), NGC 4151 (Penston & Perez 1984), Fairall 9 (Kollatschny & Fricke 1985), Mrk 1018 (Cohen et al. 1986), Mrk 99 (Tran, Osterbrock & Martel 1992), NGC 1097 (Storchi-Bergmann, Baldwin & Wilson 1993), NGC 7582 (Aretxaga et al. 1999), NGC 2617 (Shappee et al. 2014), Mrk 590 (Denney et al. 2014), and the quasars SDSS J015957.64+003310.5

*E-mail: mlparker@ast.cam.ac.uk

(LaMassa et al. 2015) and SDSS J101152.98+544206.4 (Runnoe et al. 2016). The most extreme examples known come with dramatic changes not only in their broad Balmer lines, but also in their more narrow high-ionization lines like [Fe VII] and [Fe XIV]. Cases include IC 3599 (Brandt, Pounds & Fink 1995; Grupe et al. 1995; Komossa & Bade 1999), SDSS J095209.56+214313.3 (Komossa et al. 2008) and SDSS J074820.67+471214.3 (Wang et al. 2011). More recent studies have begun to look at small samples of changing look AGN (Ruan et al. 2015; MacLeod et al. 2016; Runco et al. 2016).

There are several potential causes for rapid changes in the (apparent) brightness of AGN. In the unified model of AGN, the differences between Seyfert 1 and Seyfert 2 galaxies are interpreted as being largely due to the effect of inclination, with the inclination of Seyfert 2 AGN being such that the torus obscures the inner regions, strongly absorbing the X-ray emission and blocking the broad line region (BLR) from the observer. When the observer's line of sight skims the edge of the torus, rapid changes in the observed flux can occur when obscuring clouds at the edge of the torus move to allow a clear view of the central regions of the AGN (e.g. Goodrich 1989; Antonucci 1993; Leighly et al. 2015). However, it is challenging to attenuate a large fraction of the light from the BLR with this mechanism, as this requires different parts of the extended torus to act simultaneously. Alternatively, these events could be caused by large changes in the accretion rate of the AGN, with a large increase in the accretion rate correspondingly increasing the AGN luminosity (e.g. Nicastro 2000; Korista & Goad 2004; Elitzur, Ho & Trump 2014; Runnoe et al. 2016). Finally, stellar tidal disruption events (TDEs; Rees 1988; Komossa 2015) could cause a sudden increase in brightness. Systematic searches for changing look AGN in quasars suggest that the majority are related to changes in the accretion rate (Ruan et al. 2015) and >15 per cent of strongly variable luminous quasars show such variability on time-scales of 8–10 yr (MacLeod et al. 2016), although the sample sizes in these studies are relatively small.

In this work we present *XMM–Newton*, *NuSTAR*, and SALT observations of the flaring AGN HE 1136-2304, with the aim of establishing the cause of the outburst and its change in Seyfert type. HE 1136-2304 is a nearby, relatively unknown AGN at redshift $z = 0.027$ (Reimers, Koehler & Wisotzki 1996, RA: $11^{\rm h}38^{\rm m}51\overset{\rm s}{.}1$ DEC: $-23^{\rm d}21^{\rm m}36^{\rm s}$). It was detected in X-rays in the ROSAT All-Sky Survey (RASS; Voges et al. 2000) and is a faint radio source (8.2 mJy; Condon et al. 1998).

Throughout this paper, we assume a cosmology with $H_0 = 70\,{\rm km\,s^{-1}\,Mpc^{-1}}$, $\Omega_\Lambda = 0.73$ and $\Omega_{\rm M} = 0.27$.

2 OBSERVATIONS AND DATA REDUCTION

2.1 X-ray observations

The X-ray observations presented here are based off *XMM–Newton* (Jansen et al. 2001) proposal ID 74126 (PI N. Schartel), *'Outbursts of Radio-Quiet AGN'*. This proposal was intended to obtain an observation of a flaring AGN, and as such had a triggering condition that the source flux had to be in excess of 15 times the flux observed with *ROSAT*. HE 1136-2304 was initially detected in outburst using the *XMM–Newton* Slew Survey in 2010, at a flux ratio of 13.3 ± 2.0. While significantly above the *ROSAT* level, this did not meet the required flux level. However, follow up observations with *Swift* found that the source reached a flux level of ∼16 times that found by *ROSAT*, representing a genuine outburst, and a peak flux ratio of ∼30 was later found with *Swift*. Based on this detection, we triggered the simultaneous observations with *XMM–Newton* and *NuSTAR* (Harrison et al. 2013). The flux ratios for all observations are given in Table 1. We note that the source was also detected in the *Swift* BAT 70-month catalogue, with an average 14–195 keV flux of $17^{+22}_{-11} \times 10^{-12}$ erg s^{-1} cm^{-2}.

We used the *XMM–Newton* Science Analysis Software (SAS) version 14.0.0 to reduce the *XMM–Newton* data, extracting EPIC-pn (Strüder et al. 2001) and MOS (Turner et al. 2001) event files using EPPROC and EMPROC respectively. Both the EPIC-pn and MOS detectors were operated in small window mode. We filter for background flares, and extract source and background spectra from 30 arcsec circular extraction regions, choosing the background region so as to avoid contaminating photons from HE 1136-2304 or other objects in the field of view. We use the SPECGROUP tool to rebin the spectra to a signal-to-noise ratio of 6 and oversampling the instrumental resolution by a factor of 3, ensuring the applicability of χ^2 statistics. A preliminary investigation of the reflection grating spectrometer (RGS) spectra reveals no highly significant features, so we restrict our analysis to the lower resolution, higher sensitivity detectors.

The *NuSTAR* data were reduced using the *NuSTAR* Data Analysis Software (NUSTARDAS) version 1.4.1 and the CALDB version 20150316 (more recent versions at the time of writing only update the *NuSTAR* clock correction file, so will not affect our results). Spectra and light curves were extracted with the NUPRODUCTS tool, using 60 arcsec circular extraction regions. As with the *XMM–Newton* spectra, the *NuSTAR* spectra are binned to oversample the data by a factor of 3 and a signal-to-noise ratio of 6. We fit the *NuSTAR* spectra over the whole band (3–79 keV). The details of these observations, and those of *XMM–Newton*, are given in Table 2, and the fluxes are plotted in Fig. 1.

All X-ray spectra are fit using XSPEC version 12.8.2l, and all errors are reported at 1σ unless otherwise stated. We assume Galactic absorption of 3.82×10^{20} cm^{-2} (Willingale et al. 2013), and use the abundances of Wilms, Allen & McCray (2000).

2.2 Optical spectroscopy with the SALT telescope

To determine if the X-ray flare corresponded to a changing look in the optical band, we observed HE 1136-2304 with the 10 m Southern African Large Telescope (SALT) nearly simultaneously to the XMM observations on 2014 July 7 under photometric conditions. The optical spectrum was taken with the Robert Stobie Spectrograph attached to the telescope using the PG0900 grating with a 2.0 arcsec wide slit. We covered the wavelength range from 4203 to 7261 Å at a spectral resolution of 6.5 Å (FWHM) and a reciprocal dispersion of 0.98 Å pixel^{-1}. The observed wavelength range corresponds to a wavelength range from 4078–7050 Å in the rest frame of the galaxy. There are two gaps in the spectrum caused by the gaps between the three CCDs: one between the blue and the central CCD chip as well as one between the central and red CCD chip covering the wavelength ranges 5206.5–5262.7 Å and 6254.4–6309.1 Å (5079–5135 Å and 6100–6150 Å in the rest frame). The seeing was 1.1 arcsec, and the exposure time was 2 × 600 s (20 min).

In addition to the galaxy spectrum, necessary flat-field and Xe arc frames were also observed, as well as a spectrophotometric standard star for flux calibration (LTT4364). The spectrophotometric standard star was used to correct the measured counts for the combined transmission of the instrument, telescope and atmosphere as a function of wavelength. Flat-field frames were used to correct for differences in sensitivity both between detector pixels and across the field. The spatial resolution per binned pixel is 0.2534 arcsec for our SALT spectrum. We extracted seven columns from our object spectrum corresponding to 1.77 arcsec.

Table 1. *ROSAT* PSPC, *XMM–Newton* EPIC-pn and *Swift* XRT fluxes for HE 1136-2304.

Instrument	Date	Count rate[a]	0.2–2 keV flux	Ratio
ROSAT	1990	0.042 ± 0.015	0.4 ± 0.2	1
XMM–Newton (slew)	2007-01-12	<1.5	<2.1	<5.3
XMM–Newton (slew)	2010-01-03	3.7 ± 0.6	5.3 ± 0.8	13.3 ± 2.0
XMM–Newton (slew)	2011-12-10	2.0 ± 0.5	2.9 ± 0.7	7.3 ± 1.7
XMM–Newton (slew)	2014-06-06	3.3 ± 0.9	4.7 ± 1.2	11.8 ± 3.1
$Swift_{initial}$ (PC)	2014-06-25	0.46 ± 0.02	6.2 ± 0.3	15.5 ± 1.3
XMM–Newton	2014-07-02	2.67 ± 0.01	4.32 ± 0.01	10.8 ± 0.03
$Swift_{max}$ (WT)	2014-08-01	0.93 ± 0.04	11.6 ± 0.5	29 ± 1

Note. Fluxes are in units of 10^{-12} erg s^{-1} cm^{-2}, and are calculated using model 2 from Table 3, including the effect of absorption. Ratios are relative to the *ROSAT* flux. [a]Energy bands for the count rates differ between instruments. For *XMM–Newton*, all rates are from 0.2–2 keV. For *ROSAT*, the count rate is from 0.1–2.4 keV, and for *Swift*, the count rate is from 0.3–10 keV.

Table 2. Observation details for the *XMM–Newton* and *NuSTAR* detectors.

Instrument	Obs ID	Start time (UTC)	End time (UTC)	Clean exposure time (ks)	Count rate (s^{-1})
EPIC-pn	0741260101	2014-07-02 08h08m	2014-07-03 13h56m	71.11	3.743 ± 0.007
EPIC-MOS1	0741260101	2014-07-02 08h02m	2014-07-03 13h52m	97.20	0.876 ± 0.003
EPIC-MOS2	0741260101	2014-07-02 08h03m	2014-07-03 13h52m	97.02	1.165 ± 0.003
FPMA	80002031002	2014-07-02 08h16m	2014-07-02 22h31m	23.81	0.308 ± 0.004
	80002031003	2014-07-02 22h31m	2014-07-04 10h01m	63.57	0.255 ± 0.002
FPMB	80002031002	2014-07-02 08h16m	2014-07-02 22h31m	23.80	0.292 ± 0.004
	80002031003	2014-07-02 22h31m	2014-07-04 10h01m	63.52	0.245 ± 0.002

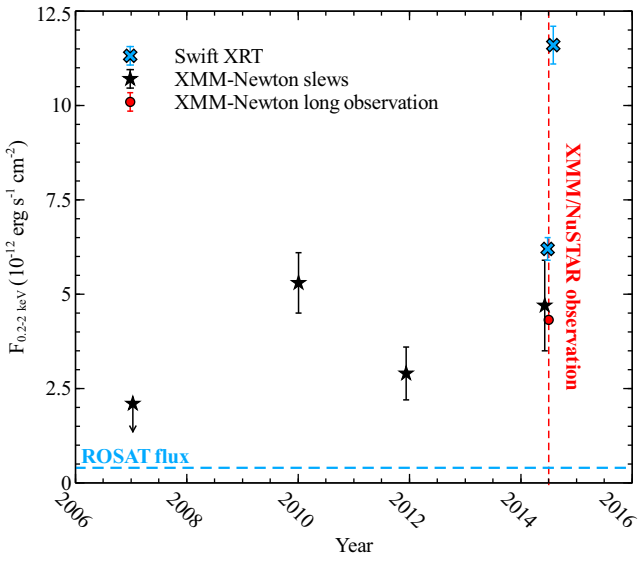

Figure 1. Long-term light curve showing the fluxes from Table 2. The 1990 *ROSAT* flux is shown by the horizontal dashed line and the time of the joint *XMM–Newton*/*NuSTAR* observation is shown by the vertical dashed line. The SALT spectrum was taken 3 d after the end of the *NuSTAR* observation.

The reduction of the spectra (bias subtraction, cosmic ray correction, flat-field correction, 2D-wavelength calibration, night sky subtraction, and flux calibration) was done in a homogeneous way with IRAF reduction packages (e.g. Kollatschny et al. 2001). We corrected the optical spectra of HE1136-2304 for Galactic extinction. We used the reddening value $E(B-V) = 0.036\ 66$ deduced from the Schlafly & Finkbeiner (2011) re-calibration of the Schlegel, Finkbeiner & Davis (1998) infrared-based dust map. The reddening law of Fitzpatrick (1999) with $R_V = 3.1$ was applied to our spectra. All wavelengths were converted to the rest frame of the galaxy ($z = 0.027$).

3 RESULTS

3.1 X-ray spectrum

We run a series of tests on the X-ray spectrum of HE 1136-2304, using the excellent broad-band data to try and shed light on the nature of the changes in the optical spectrum. We look for changes in the flux and spectral shape within the observations, which may indicate what dominates the variability on short time-scales, we search for the signatures of absorption (either ionized or neutral) in the spectrum, and fit the spectrum with various models that can be used to compare it to other, similar, AGN.

In Fig. 2 we show the *XMM–Newton* and *NuSTAR* light curves over the whole observation. A ∼30 per cent drop in flux is immediately obvious in the *XMM–Newton* EPIC-pn light curve, which declines smoothly over around 25–75 ks. A similar, though less strong, drop is also observed in the *NuSTAR* light curve, which declines by around 25 per cent. The high and low flux intervals are (coincidentally) neatly divided by the two *NuSTAR* observation IDs, so the high energy spectral evolution, if present, should be visible in the difference between the two spectra.

While there is very little short-term variability in the light curve (Fig. 2, left), there is a ∼30 per cent drop in flux in the 0.3–10 keV band over the course of the *XMM–Newton* observation. In the right-hand panel of Fig. 2 we show the ratio of the EPIC-pn spectrum to an absorbed power law for the two halves of the *XMM–Newton* observation, allowing for a difference in normalization between the two. It is apparent from this that there is no significant change in spectral shape corresponding to the drop in flux. The only potential difference is a slight increase in the iron line residuals, as would be expected if the narrow line originates far from the X-ray

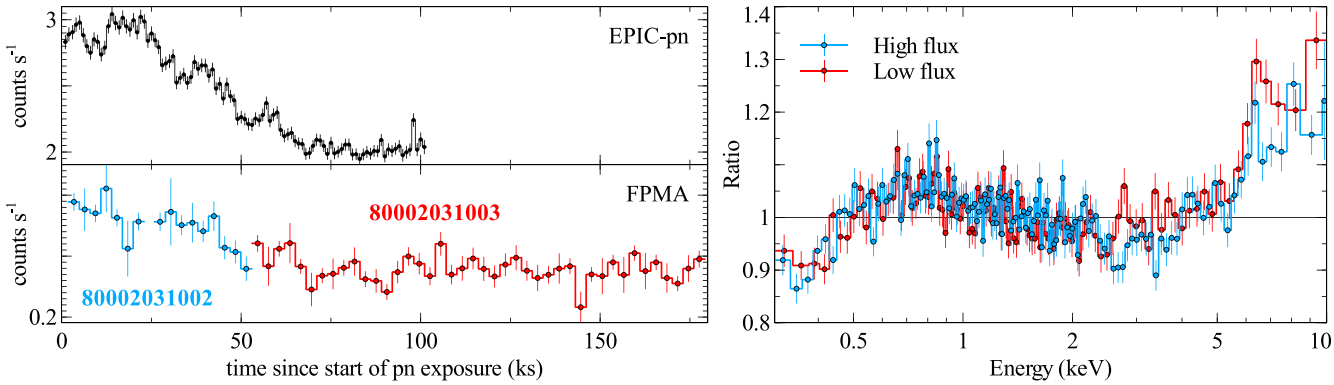

Figure 2. Left: background subtracted *XMM–Newton* EPIC-pn and *NuSTAR* FPMA light curves over the whole energy range, binned to 1 and 3 ks, respectively. The two *NuSTAR* observation IDs are plotted separately, in red and blue. Right: ratio of the EPIC-pn data to an absorbed power law for the two halves (high and low flux) of the *XMM–Newton* observation, showing the absence of spectral changes with flux.

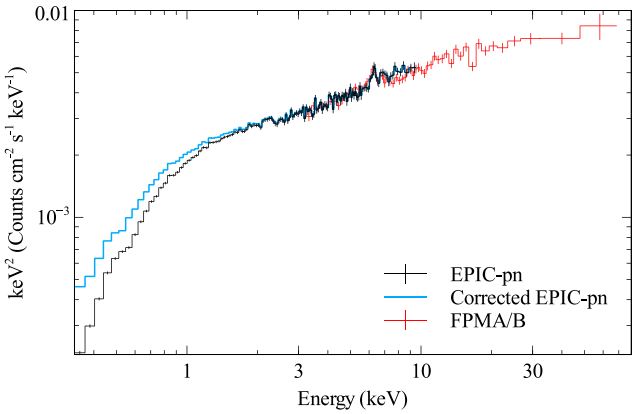

Figure 3. Unfolded *XMM–Newton* and *NuSTAR* spectrum of HE 1136-2304 to a power law with $\Gamma = 0$. The blue line shows the EPIC-pn points after correcting for Galactic absorption. It is obvious from this that there is additional absorption intrinsic to the source.

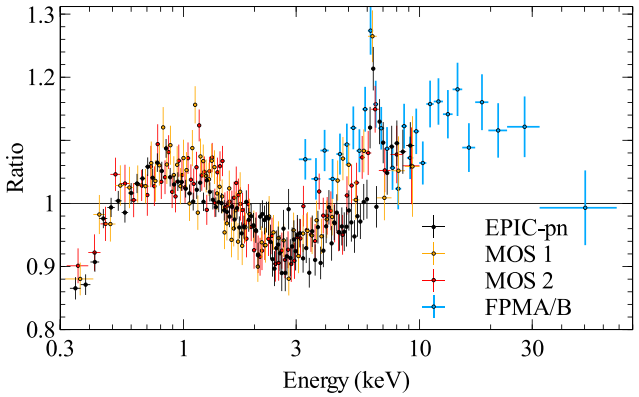

Figure 4. Ratio of the X-ray spectrum to an absorbed power law, fit from 0.3–80 keV. The soft excess, iron line and hard excess/cutoff are all clearly visible. *NuSTAR* FPMA and FPMB data are grouped in XSPEC and all spectra are rebinned for clarity.

continuum source and therefore responds slowly. Because of the lack of spectral evolution, we combine the two *NuSTAR* observations into a single spectrum for each of the two FPMs, and fit all the data simultaneously.

In Fig. 3 we show the EPIC-pn and focal plane module (FPM) A/B spectra, unfolded to a $\Gamma = 0$ power law. The spectrum is fairly hard, and shows significant line emission around 6.4 keV. We also show the pn spectrum after correcting for Galactic absorption. A decrease in flux at low energies is still apparent, implying that there is a significant absorbing column intrinsic to the source. We next examine the residuals after taking into account this additional absorption. In Fig. 4 we show the ratio of the broad-band X-ray spectrum to the same absorbed power law, including both Galactic and intrinsic absorption (*tbabs*×*ztbabs*×*powerlaw* as an XSPEC model, i.e. Galactic absorption×intrinsic absorption×power law). A strong narrow line is clearly visible at 6.4 keV, along with a soft excess and a turnover in the *NuSTAR* band.

From the EPIC-pn spectrum alone, it appears that there may be some additional complexity around the 6.4 keV iron line, most noticeably an apparent emission line at ∼7 keV. This could potentially be due to the iron Kβ line, or could be due to an absorption feature superimposed on a broader emission line. To probe the iron line region in more detail, we use a simple line search over the 4–9 keV band, following the method outlined in Tombesi et al. (2010) and assuming a power-law continuum. The results are shown in Fig. 5. We perform the search separately for each set of detectors, then in a combined fit, so that detections can be compared between instruments. In all cases, we find the 6.4 keV line to be highly significant, with the only other feature significant at the 3σ level being a spurious feature at ∼5.5 keV in the EPIC-pn, which does not correspond to any features in the other instruments. There is a general trend towards an excess at the high energy side of the iron line, which may correspond to presence of an additional line or lines, a broad component, or be due to the presence of a 7 keV absorption edge. There are various features significant at the 2σ level above 7 keV in the combined analysis (including *NuSTAR*, and MOS), however they are not consistent in size or energy and most likely correspond to the continuum over-predicting the flux in this band (we note that this method is extremely sensitive to the choice of baseline model; Zoghbi et al. 2015). The absence of any apparent ionized absorption (either warm absorber or ultra-fast outflow) in this source is interesting, and may be relevant to the change in Seyfert classification. In particular, it implies that either there is a weak or absent disc wind or that we are observing the source at such an angle that the wind does not intercept the line of sight.

We fit the combined X-ray spectrum with a variety of models, with the aim of measuring the level of the intrinsic absorption and for easy comparison with other sources. The fit results are shown in

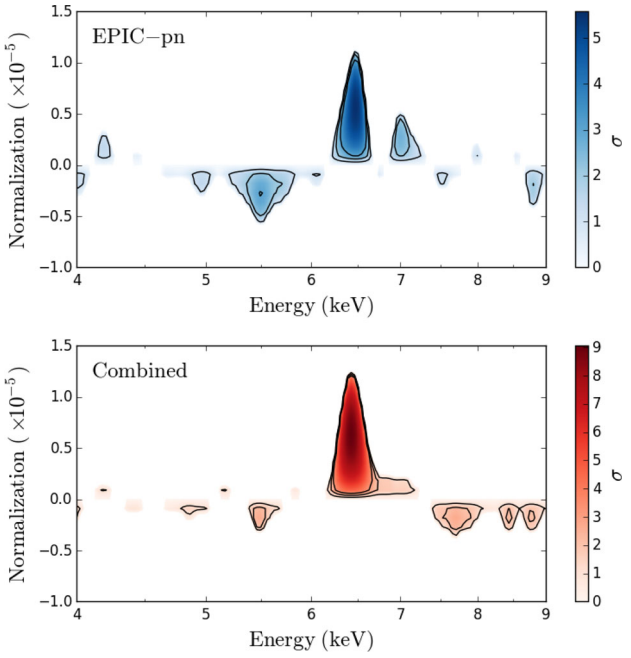

Figure 5. Results of the search for emission and absorption lines, over the 4–9 keV band. The first plot shows the results for the EPIC-pn individually, and the combined plot shows the results from fitting all five instruments (pn, MOS1/2 and FPMA/B) simultaneously. Contour lines show the 1σ, 2σ and 3σ confidence levels. Normalizations are in units of photons cm^{-2} s^{-1} and energy values are in the rest frame. The 7 keV line that appears in the EPIC-pn spectrum is not significant when the other data is taken into account.

Table 3. In all fits we allow for a normalization offset between the five detectors. The following models are used.

(i) Model 1: Fitting *XMM–Newton* data from 0.3–2 keV with an absorbed (Galactic and intrinsic absorption) power law. This model is for comparison with the *ROSAT* and *XMM–Newton* slew surveys, which fit models over similar bands.

(ii) Model 2: As model 1, but fit up to 10 keV, again only using *XMM–Newton* data and including a narrow emission line at 6.4 keV. This model allows for more general comparison with *XMM–Newton* (and other) observed AGN.

(iii) Model 3: As model 2, but now including a soft excess, modelled with a blackbody (*bbody* in XSPEC). We test adding both neutral (modelled using *zpcfabs*) and ionized (modelled using *zxipcf*, Reeves et al. 2008) partially covering absorbers, and find no improvement to the fit from adding either.

(iv) Model 4: As model 3, but now including the *NuSTAR* data from 3–79 keV, and replacing the power law with a cut-off power law (*cutoffpl*). Again, we try including additional partial covering absorption and find no improvement to the fit. This is our best-fitting phenomenological model, which includes spectral components to describe all major features of the spectrum.

(v) Model 5: A more physical model, where we replace the narrow Gaussian line with a distant reflection component modelled with *xillver* (García & Kallman 2010), and use a combination of Comptonization (*comptt*; Titarchuk 1994) and relativistic reflection (*relxill*; García et al. 2014) to fit the soft excess and broad-band spectral curvature. We use a broken power-law emissivity profile, fixing the outer index at 3, and the break radius at $6R_G$. Removing either of the reflection and Comptonization components worsens the fit significantly ($\Delta\chi^2 \sim 50$), although it is not entirely clear what spectral features this is due to in the reflection case. It is most likely required to fit subtle spectral curvature in the high-quality broad-band spectrum. As with the other models, additional absorbers do not improve the fit significantly.

Models 1–4 are phenomenological, and are intended for comparison purposes. We show the residuals to the best-fitting models 4

Table 3. X-ray spectral fit parameters for the different models. Models 1–4 are phenomenological, and model 5 is made up of physical components. Models 1–3 are fit to different subsets of the data.

Parameter	Value	Units	Description
Model 1 – *tbabs*×*ztbabs*×*(powerlaw)* – (0.3–2 keV)			
n_H	1.50 ± 0.03	10^{21} cm^{-2}	Column density
Γ	2.00 ± 0.02		Power-law index
χ^2/d.o.f.	282/150=1.88		
Model 2 – *tbabs*×*ztbabs*×*(powerlaw+zgauss)* – (0.3–10 keV)			
n_H	1.09 ± 0.01	10^{21} cm^{-2}	Column density
Γ	1.764 ± 0.004		Power-law index
E_{Gauss}	6.421 ± 0.003	keV	Line energy
χ^2/d.o.f.	1468/504=2.91		
Model 3 – *tbabs*×*ztbabs*×*(bbody+powerlaw+zgauss)* (0.3–10 keV)			
n_H	0.95 ± 0.03	10^{21} cm^{-2}	Column density
Γ	1.60 ± 0.01		Power-law index
E_{Gauss}	6.44 ± 0.01	keV	Line energy
kT	0.24 ± 0.01	keV	Blackbody temp.
χ^2/d.o.f.	764/502=1.52		
Model 4 – *tbabs*×*ztbabs*×*(bbody+cutoffpl+zgauss)* (0.3–79 keV)			
n_H	0.94 ± 0.03	10^{21} cm^{-2}	Column density
Γ	1.57 ± 0.02		Power-law index
E_{cut}	102^{+23}_{-16}	keV	Cut-off energy
E_{Gauss}	6.43 ± 0.01	keV	Line energy
kT	0.24 ± 0.01	keV	Blackbody temp.
χ^2/d.o.f.	1144/851=1.34		
Model 5 – *tbabs*×*ztbabs*×*(comptt+cutoffpl+xillver+relxill)* (0.3–79 keV)			
n_H	1.55 ± 0.01	10^{21} cm^{-2}	Column density
Γ	<1.43		Power-law index
E_{cut}	40^{+6}_{-2}	keV	Cut-off energy
T_0	$0.93^{+0.02}_{-0.03}$	keV	Seed temp.
kT	<1.9	keV	Plasma temp.
τ	$6.7^{+0.2}_{-0.4}$		Optical depth
A_{Fe}	>9		Iron abundance
q_{in}	>8.5		Emissivity index
i	78^{+2}_{-1}	degrees	Inclination
a	>0.995		Spin
log (ξ)	2.4 ± 0.1	erg cm s^{-1}	Ionization
χ^2/d.o.f.	1028/841=1.22		
Cross-normalization constants (relative to EPIC-pn)			
C_{MOS1}	0.859 ± 0.003		
C_{MOS2}	1.036 ± 0.004		
C_{FPMA}	1.06 ± 0.01		
C_{FPMB}	1.09 ± 0.01		
Luminosities (EPIC-pn)			
L(0.5–2)	1.15×10^{43}	erg s^{-1}	
L(2–10)	1.69×10^{43}	erg s^{-1}	

Note. Luminosities and normalization constants are calculated from model 5, and luminosities are corrected for absorption (both Galactic and intrinsic).

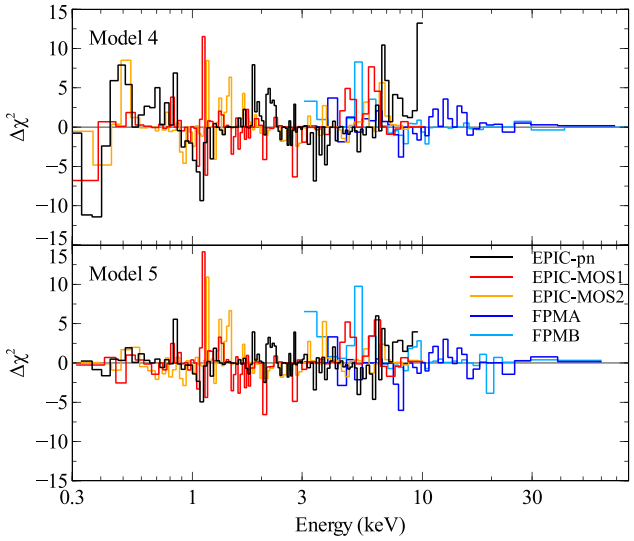

Figure 6. χ^2 residuals for the best-fitting phenomenological and physical models (top and bottom, respectively). Different colours correspond to the five different instruments. A disagreement between the MOS and pn detectors is seen just above 1 keV, and a slightly different slope is found between the FPMs and the EPIC instruments between 3 and 10 keV. Aside from these instrumental effects, there are no significant residuals in the physical model. The phenomenological model shows strong residuals around the soft excess. The corresponding models are shown in Fig. 7.

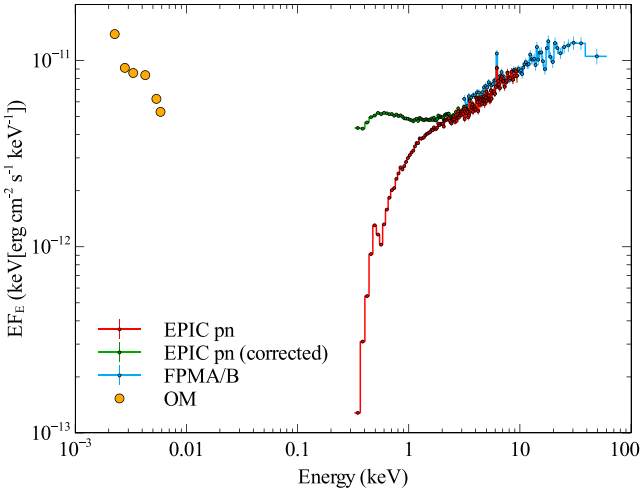

Figure 8. *XMM–Newton* and *NuSTAR* SED. Green points show the EPIC-pn spectrum after correcting for both Galactic and intrinsic absorption.

and 5 in Fig. 6, and the models themselves in Fig. 7. For model 4, the main residual features are at low energies, and presumably arise from our phenomenological model of the soft excess. There is a small disagreement in Γ between the *XMM–Newton* and *NuSTAR* instruments from 3–10 keV, which also contributes to the relatively high χ^2 values we find. For model 5, the main residuals are around 1 keV, where there is a disagreement between the MOS and pn detectors, and from 3–10 keV, where the *NuSTAR* and *XMM–Newton* spectra overlap.

We can estimate from the best-fitting model (model 5) the column density that would be needed to reduce the X-ray flux to the level observed in 1990. By adjusting the column density of the neutral absorber at the source redshift (*ztbabs*), we find that the column density needed is $\sim 2.45 \times 10^{22}$ cm^{-2}, compared to the observed 1.5×10^{21} cm^{-2} in 2014. However, the column density measured in the 2014 observations is not sufficient to explain the rise in flux to the highest flux *Swift* XRT observation. The XRT maximum 0.2–2 keV flux is more than twice that found with *XMM–Newton*, and removing the absorber completely only produces a 50 per cent increase in flux. This suggests that the majority of the short term X-ray variability is intrinsic to the source.

In Fig. 8 we show the SED of HE 1136-2304 from 2014-07-02 with the *XMM–Newton* EPIC-pn and optical monitor (OM), and *NuSTAR*. We also show the effect of the absorption, by correcting the EPIC-pn spectrum for both intrinsic and Galactic absorption. It is clear from this that a large fraction of the flux is being emitted in the X-rays.

3.2 Optical spectrum

The optical spectrum of HE1136-2304 taken with the SALT telescope in 2014 is presented in Fig. 9. This spectrum is shown in

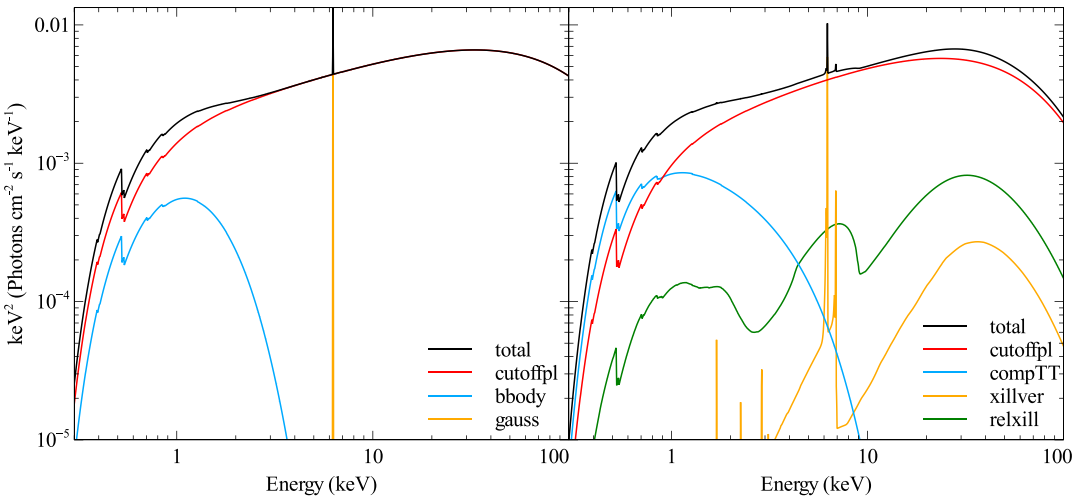

Figure 7. Best-fitting broad-band spectral models, showing the different spectral components used. Left and right plots correspond to the phenomenological and physical models, respectively. In both cases, the spectrum is dominated by the continuum power law, with a strong narrow iron line.

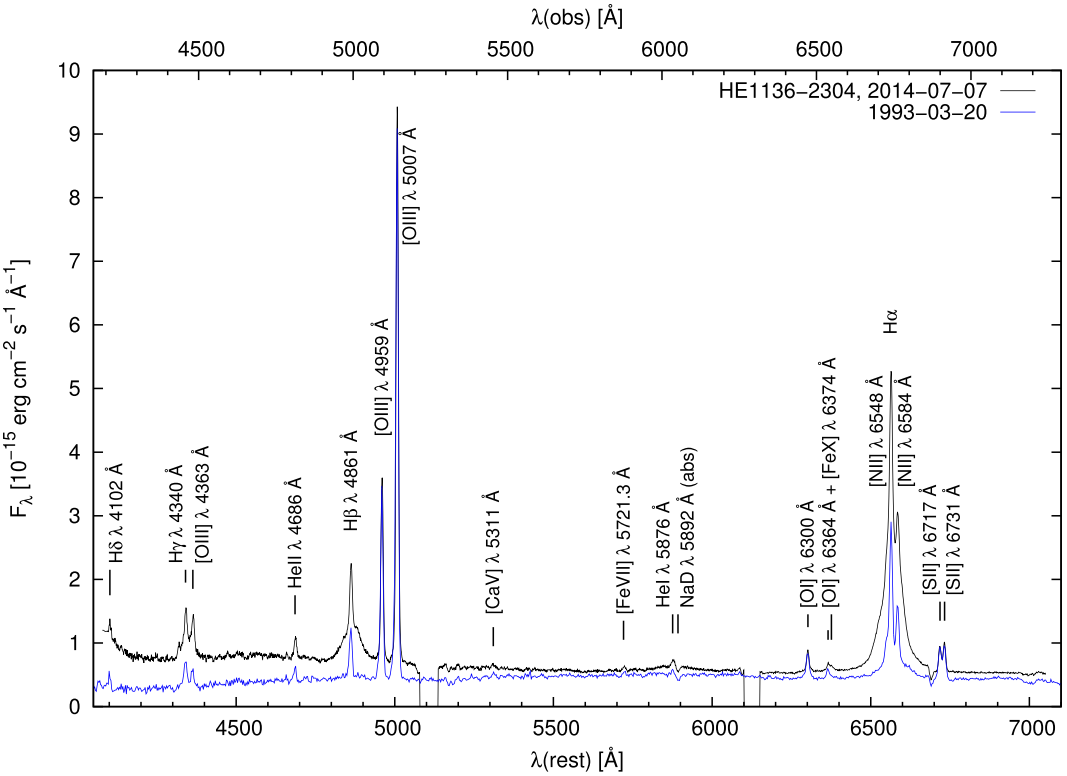

Figure 9. Optical spectrum of HE1136-2304 taken with the SALT telescope on 2014 July 7 (black line). A further spectrum of this AGN taken in 1993 (blue line) is overlayed for comparison. The broad Hα and Hβ lines are clearly much stronger in the 2014 spectrum than in the 1993 spectrum.

the rest frame of the AGN. Based on this observed spectrum we calculate a blue magnitude m_B of 17.3 ± 0.1 for HE 1136-2304.

We derived the flux of the emission line intensities by integrating the flux above a linearly interpolated continuum, locally defined by regions just bluewards and redwards of the individual emission lines. The fluxes were integrated for the wavelength ranges given in column 3. We present in Table 4 the observed emission line intensities as well as those corrected for Galactic extinction.[1] With respect to the relative intensities of the broad and narrow Balmer line components, for example Hβ, HE 1136-2304 has to be classified as Seyfert 1.5 type based on its spectrum taken in July 2014. This is based on the definition of Osterbrock & Ferland (2006) that Seyfert galaxies with intermediate-type H I profiles in which both components can easily be recognized are of Seyfert type 1.5.

The relative intensities of the highly ionized lines are quite strong. The [Fe X]λ6374 line intensity, for example, is stronger in HE 1136-2304 than in the prototype Seyfert 1.5 galaxy NGC 5548 (Peterson et al. 1994). The narrow lines, for example [O III]λ5007, hold line widths (FWHM) of 510 ± 10 km s^{-1}. The broad Hβ component shows a width of 4200 ± 200 km s^{-1}. These values are typical for Seyfert galaxies. We determined the line widths in units of km s^{-1} by converting our spectrum into velocity space with the IRAF task 'disptrans'. This broad component of Hβ is redshifted with respect to the narrow component by 250 ± 50 km s^{-1}.

[1] Note that we have neglected a possible weak Fe II component in our optical spectra which will overlap with the [O III] and Hβ lines. Given how bright these lines are relative to the Fe II component, this contamination is negligible. Additionally, the relative flux contribution of the [N II] lines with respect to the Hα-[N II] line complex is far stronger in the faint state, introducing additional uncertainty into the measurements of the Hα fluxes.

Table 4. Rest-frame optical emission line intensities of HE1136-2304 from 2014: observed values (2) and corrected for Galactic extinction (3).

Emission line	Flux		Wavelength range
	Obs.	Corr.	
(1)	(2)	(3)	(4)
Hγ	20 ± 2	24.5 ± 2	4311 – 4386
[O III] λ4363	5.5 ± 1	6.2 ± 1	4353 – 4374
He II λ4686	3.3 ± 0.1	4.3 ± 0.1	4674 – 4698
Hβ (broad)	40 ± 5	43 ± 5	4782 – 4936
Hβ (narrow)	9 ± 2	10 ± 2	4850 – 4871
[O III] λ4959	27 ± 2	31 ± 2	4940 – 4979
[O III] λ5007	83 ± 3	91 ± 3	4984 – 5027
[Ca V] λ5311	0.7 ± 0.2	0.8 ± 0.2	5300 – 5321
[Fe VII] λ5721	0.8 ± 0.1	0.9 ± 0.1	5712 – 5733
He I λ5876	1.4 ± 0.1	1.6 ± 0.1	5864 – 5887
[O I] λ6300	3.9 ± 0.5	4.2 ± 0.5	6279 – 6320
[O I] λ6364	1.4 ± 0.3	1.5 ± 0.3	6348 – 6373
[Fe X] λ6374	0.93 ± 0.2	0.95 ± 0.3	6373 – 6396
Hα (broad, incl.[*N ii*])	191 ± 25	211 ± 25	6400 – 6670
Hα (narrow)	20 ± 2	22 ± 2	6556 – 6572
[N II] λ6584	7.6 ± 1	7.8 ± 1	6576 – 6598
[S II] λ6717	4.3 ± 0.4	4.4 ± 0.5	6706 – 6725
[S II] λ6731	4.5 ± 0.4	5.0 ± 0.5	6725 – 6745

Note. Line fluxes (2) in units of 10^{-15} erg s^{-1} cm^{-2}.

We use the flux variation gradient (FVG) method (Choloniewski 1981; Winkler et al. 1992; Pozo Nuñez et al. 2015) to estimate the relative contributions of the host and AGN to the continuum flux (shown in Fig. 10). We calculate *B* and *R*-band fluxes for each spectrum by convolving them with *B* and *R* filter curves. From 1993 to 2014 the *R*-band flux increases from 0.73 ± 0.04 to 0.89 ± 0.02 and

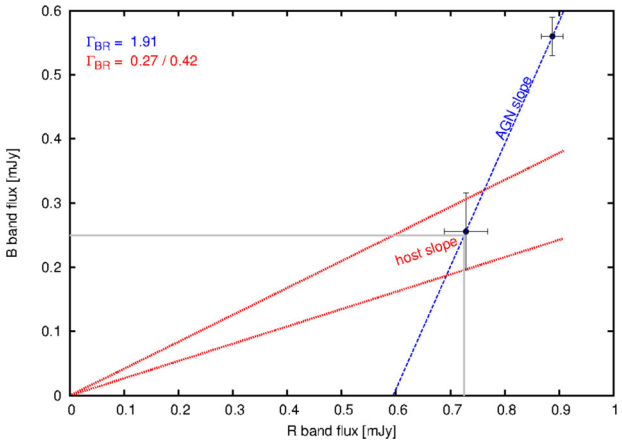

Figure 10. *B* versus *R* flux variations of He1136-2304. The two measurements of He1136-2304 in the bright state (2014) and in the low state (1993) are used to determine the AGN slope (blue). The red dashed lines give the range of host slopes for nearby AGN as determined by Sakata et al. (2010). The intersections between the AGN and host galaxy slopes gives the possible range of host galaxy fluxes in the *B* and *R* bands (grey lines indicate the central value of $R = 0.73$ mJy, $B = 0.25$ mJy).

the *B*-band from 0.26 ± 0.06 to 0.56 ± 0.03. The AGN and host flux lines intercept at *R* and *B* band fluxes of 0.73 mJy and 0.25 mJy, respectively. From this, we can infer that the maximum contribution of the AGN to the blue continuum in 1993 was ∼20 per cent, and that it must have increased by a factor of at least 4 in 2014. Similarly, the 1993 broad Hα and Hβ line fluxes were $(55 \pm 10) \times 10^{-15}$ erg s^{-1} cm^{-2} and $(15 \pm 5) \times 10^{-15}$ erg s^{-1} cm^{-2}, a factor of 3–4 below those measured in 2014. A caveat here is that the two spectra were taken with different aperture sizes, so may contain slightly different host galaxy contributions.

Based on the column density needed to lower the X-ray flux to the level of 1990 ($\sim 2.45 \times 10^{22}$ cm^{-2}, see Section 3.1), we can estimate the corresponding effect that the associated reddening should have had on the blue continuum flux, in the case that a drop in the absorbing column is the cause of the X-ray flare. Converting the column density to extinction using the relation from Predehl & Schmitt (1995) and assuming $A_V = 3.1 E_{B-V}$, we find that the flux at 5500 Å should be lower by a factor of $\sim 10^5$ with respect to the 2014 flux. We note that in AGN the ratio of A_V to $N_{\rm H}$ is generally significantly lower than that from Galactic absorption: Maiolino et al. (2001) find that most AGN have $A_V/N_{\rm H}$ a factor of 10 lower than Galactic, with some up to 100 times lower. Lowering the A_V values by 10 and 100 corresponds to flux ratios ($F(2014)/F(1993)$) of 46 and 1.5, respectively.

The high-amplitude variability of HE 1136-2304 makes BH mass estimates more uncertain. For a first order of magnitude estimate, we use the optical continuum luminosity, which varied very little. Using the width of the broad Hβ line, continuum luminosity ($\log [\lambda L_\lambda (5100\,\text{Å})] = 42.72 \pm 0.05$) and the mass scaling relation of Vestergaard & Peterson (2006, equation 5) we find a black hole mass of $\log (M_{\rm BH}/{\rm M}_\odot) = 7.3 \pm 0.4$ in 2014 and 6.9 ± 0.5 in 1993, assuming 50 per cent and 10 per cent of the luminosity at 5100 Å is due to the AGN, respectively, based on the FVG results. Assuming a bolometric luminosity of $L_{\rm bol} \approx 9 \lambda L_\lambda (5100\,\text{Å}) = 2.3 \times 10^{43}$ erg s^{-1} in 2014 (Kaspi et al. 2000) we find an Eddington fraction of ∼0.01. This may be an underestimate, however, as the 0.5–10 keV X-ray luminosity is $\sim 2.8 \times 10^{43}$ erg s^{-1}, which would suggest the bolometric luminosity should be significantly larger. From the 2–10 keV luminosity (Table 3) we can calculate an alternative estimate of the bolometric luminosity of 3.4×10^{44} erg s^{-1}, assuming a bolometric correction factor of $\kappa_{2-10\rm keV} = 20$ (see Vasudevan et al. 2009). This corresponds to an Eddington fraction of ∼0.09, which is significantly higher than that found from the continuum luminosity. Note that this range of inferred Eddington fractions is on the same order as the critical accretion rate ($\dot{m}/\dot{m}_{\rm Edd} = 0.01$) required in the model of Nicastro (2000) for the onset of a significant BLR. As seen in the SED (Fig. 8) the X-ray flux is relatively high, which explains the difference in results found here.

For an independent estimate of the historical X-ray emission, we have used the [O III] emission from the narrow-line region Table 4. Based on the correlation between [O III] luminosity and (2–10) keV X-ray luminosity of Lamastra et al. (2009), and the observed [O III] luminosity of HE 1136-2304, we predict an X-ray luminosity of 1.2×10^{42} erg s^{-1}, which is a factor of 14 lower than the one measured during the deep *XMM–Newton* observation (Table 3).[2] This provides independent evidence that HE 1136-2304 is currently undergoing an epoch of enhanced X-ray emission.

4 DISCUSSION

While the 2014 optical and X-ray data are simultaneous within a few days, an important caveat for the following discussion is that the earlier archival data are not simultaneous. There is a three year gap between the two, which is long enough for dramatic changes to occur in both the X-ray and optical bands, meaning that the observed fluxes and spectra are not necessarily identical to those in the corresponding band at the time of the other observation.

We fit the X-ray spectra with a variety of phenomenological models, all of which agree that a significant absorbing column (around 10^{21} cm^{-2}) is required in addition to Galactic absorption, although in no case does it greatly exceed this value. The spectrum is fairly conventional for a Seyfert 1.5. It shows a moderate soft excess, a narrow iron line at 6.4 keV and a high energy cut-off at ∼100 keV (*NuSTAR* has been shown to be capable of accurately constraining cut-off energies outside the energy band; e.g. Matt et al. 2015; Garcia et al. 2015). This cut-off energy is fairly low, but not exceptional (Fabian et al. 2015). Based on the two EPIC-pn spectra shown in the right-hand panel of Fig. 2, it is unlikely that absorption variability can be responsible for all of the variations in flux seen, as the ∼30 per cent drop in flux seen by *XMM–Newton* appears to be uniform across the bandpass, inconsistent with a change in the absorption column. Notably, there is a lack of ionized absorption in the form of either a warm absorber or an outflow, which may indicate a viewing angle that prevents the line of sight being intercepted by this material.

While the physical model gives the best overall fit to the X-ray spectrum, we caution that there are problems with this model. Several of the parameters are hitting their limits, particularly in the reflection model. Since no broad iron line is apparent in the spectrum it is difficult to be certain about the measured values. While the reflection component greatly improves the fit quality this may be for more complex reasons, such as a more complex continuum model being needed to properly reproduce the data.

[2] Note that we did not apply any extinction correction when estimating $L_{[\rm O\,III]}$. While we cannot estimate the BLR reddening from the optical spectrum because broad Hα is blended with [N II], the narrow Balmer-line ratio does not indicate any NLR reddening.

Table 5. Optical continuum fluxes for the years 1993 and 2014.

Wavelength [Å]	Flux (1993)	Flux (2014)
	[10^{-15} erg s^{-1} cm^{-2} Å^{-1}]	
4400	0.32 ± 0.03	0.77 ± 0.03
5500	0.48 ± 0.02	0.57 ± 0.01
6950	0.44 ± 0.01	0.53 ± 0.01

Using SALT spectroscopy we have determined that HE 1136-2304 changed its spectral type from nearly Seyfert 2 type (i.e. Seyfert 1.95) in March 1993 to a Seyfert 1.5 type in July 2014, coinciding with a huge increase in X-ray flux measured with *XMM–Newton* and *Swift*. There was only a very weak broad Hα component apparent in the optical spectrum taken in 1993 March (see optical spectrum in Reimers et al. 1996, our Fig. 9) and there was no indication for a broad Hβ component in 1993. The definition for a Seyfert 1.9 type is based on that of Osterbrock & Ferland (2006), i.e. that no broad Hβ emission can be seen in the spectrum. We scaled the spectrum taken in the year 1993 with respect to the intensity of the [O III] λ5007 line taken in 2014.

In contrast to the Balmer line and X-ray flux we did not see much change in the optical continuum flux when comparing the spectra taken in 1993 and 2014. While the general optical continuum flux strength is similar at both epochs there is a difference in the gradient, which is bluer in 2014 relative to 1993. We give in Table 5 the derived continuum intensities at three optical continuum wavelengths for the years 1993 and 2014.

There are several potential explanations for the observed increase in X-ray flux and appearance of broad lines, which we will now consider.

(i) Some *inactive* galaxies have been seen to flare due to stellar tidal disruption events (TDEs; e.g. Komossa & Bade 1999). HE 1136-2304 itself is a classical AGN, judged from its optical emission line ratios (log ([O III]5007/Hβ) = 0.96, log ([S II]6724/Hβ) = –0.35) which place it well within the AGN regime in diagnostic diagrams. While TDEs can also occur in AGN, it is more difficult to make a positive case for them in systems which permanently harbour an accretion disc, as the increase in flux is less dramatic relative to the non-flaring flux in an AGN. Further, we note that the high-state X-ray spectrum below 2 keV (Tab. 2), is rather flat, unlike the majority of soft X-ray TDEs which showed ultra-soft X-ray spectra (e.g. Bade, Komossa & Dahlem 1996). In addition, the detection of the source in *XMM–Newton* slews from 2010 and 2011 is inconsitent with a single TDE, which would follow a well established decay profile on shorter time-scales (Rees 1988, 1990).

(ii) Another idea is that there is in fact no change in the intrinsic brightness – instead, the broad lines and X-ray emission were obscured by dusty absorbing material, which left the line of sight, causing the apparent X-ray outburst and revealing the broad line region. The presence of mild absorption in the X-ray spectrum may support this, and the high inclination suggested by the reflection model is also consistent with this picture.

(iii) Nicastro (2000) suggest a model where the width of the broad lines is controlled by the accretion rate (see also Elitzur et al. 2014, who showed that the sequence of AGN from type 1 to type 2 is controlled by the bolometric luminosity). In this model the BLR is associated with a disc wind, the radius of which increases with accretion rate. Thus, as the accretion rate increases the breadth of the lines decreases, as it is determined by the Keplerian velocity at the wind radius. Below a limiting accretion rate, however, no such wind is produced, as evaporation inhibits its formation. This model could therefore explain our observations if, as seems plausible, the accretion rate of HE 1136-2304 has crossed this threshold value, causing the X-ray outburst and BLR simultaneously.

(iv) Finally, arguably the simplest explanation is a flare in the emission from the EUV and X-rays due to an increase in the accretion rate, which then excited a larger amount of broad line emission. This can potentially be triggered by disc instabilities, without the need for any external cause (e.g. Honma, Matsumoto & Kato 1991; Komossa & Bade 1999). In practice this model is difficult to distinguish from the previous scenario, but makes no assumptions on the nature of the BLR.

5 CONCLUSIONS

We have presented X-ray and optical observations of the AGN HE 1136-2304 with *XMM–Newton*, *NuSTAR*, *Swift*, and SALT. The AGN was found to have increased in X-ray flux by a factor of $\sim$30, coinciding with the appearance of broad lines in the optical spectrum (and hence a change in classification from Seyfert 1.95 to Seyfert 1.5).

We find that the X-ray spectrum requires significant absorption in excess of the Galactic column, with a column density of $\sim 10^{21}$ cm^{-2}. An increase in column density of approximately 1 order of magnitude (to 2–3 $\times$ 10^{22} cm^{-2}) would be enough to explain the lower flux observed in 1993. However, changes in the absorption cannot explain the increased flux seen by *Swift*, meaning the majority of the short-term variability must be intrinsic to the source. While this is not conclusive, as the long-term variability could be driven by a different mechanism, it favours the interpretation of the long-term change in flux as also intrinsic to the source, caused by an increase in the accretion rate.

Sources like HE 1136-2304, which show simultaneous high-amplitude variability in X-rays and optical emission lines, provide us with tight constraints on the physics behind AGN classifications and accretion variability. If other sources where the optical continuum does not respond to the X-ray changes can be identified this may help us understand the nature of disc instabilities, particularly if the relevant time-scales can be constrained. In general, radio-quiet AGN flaring in X-rays remain a relatively unexplored area, with great potential for shedding light on accretion physics.

ACKNOWLEDGEMENTS

We thank the anonymous referee for their detailed and constructive feedback. We thank Lutz Wisotzki for making available the optical spectrum of HE1136-2304 taken in 1993, and we thank Vassilis Karamanavis for a careful reading of the manuscript. MLP acknowledges financial support from the Science and Technology Facilities Council (STFC). This paper is based on observations taken with the SALT telescope. This work has been supported by DFG grant Ko 857/32-2. Based on observations with *XMM–Newton*, an ESA science mission with instruments and contributions directly funded by ESA Member States and NASA. This work made use of data from the *NuSTAR* mission, a project led by the California Institute of Technology, managed by the Jet Propulsion Laboratory, and funded by the National Aeronautics and Space Administration. This research has made use of the *NuSTAR* Data Analysis Software (NuSTARDAS) jointly developed by the ASI Science Data Center (ASDC, Italy) and the California Institute of Technology (USA). We would also like to thank Neil Gehrels for approving the *Swift*

ToO requests, and the *Swift* science operation team for performing the observations.

REFERENCES

Antonucci R., 1993, ARA&A, 31, 473
Aretxaga I., Joguet B., Kunth D., Melnick J., Terlevich R. J., 1999, ApJ, 519, L123
Bade N., Komossa S., Dahlem M., 1996, A&A, 309, L35
Brandt W. N., Pounds K. A., Fink H., 1995, MNRAS, 273, L47
Choloniewski J., 1981, Acta Astron., 31, 293
Cohen R. D., Puetter R. C., Rudy R. J., Ake T. B., Foltz C. B., 1986, ApJ, 311, 135
Collin-Souffrin S., Alloin D., Andrillat Y., 1973, A&A, 22, 343
Condon J. J., Cotton W. D., Greisen E. W., Yin Q. F., Perley R. A., Taylor G. B., Broderick J. J., 1998, AJ, 115, 1693
Denney K. D. et al., 2014, ApJ, 796, 134
Elitzur M., Ho L. C., Trump J. R., 2014, MNRAS, 438, 3340
Fabian A. C., Lohfink A., Kara E., Parker M. L., Vasudevan R., Reynolds C. S., 2015, MNRAS, 451, 4375
Fitzpatrick E. L., 1999, PASP, 111, 63
Gallo L. C. et al., 2015, MNRAS, 446, 633
García J., Kallman T. R., 2010, ApJ, 718, 695
García J. et al., 2014, ApJ, 782, 76
Garcia J. A., Dauser T., Steiner J. F., McClintock J. E., Keck M. L., Wilms J., 2015, ApJ, 808, 37
Goodrich R. W., 1989, ApJ, 340, 190
Grupe D., Beuermann K., Mannheim K., Bade N., Thomas H.-C., de Martino D., Schwope A., 1995, A&A, 299, L5
Grupe D., Komossa S., Gallo L. C., Longinotti A. L., Fabian A. C., Pradhan A. K., Gruberbauer M., Xu D., 2012, ApJS, 199, 28
Grupe D., Komossa S., Scharwächter J., Dietrich M., Leighly K. M., Lucy A., Barlow B. N., 2013, AJ, 146, 78
Grupe D., Komossa S., Saxton R., 2015, ApJ, 803, L28
Guainazzi M., 2002, MNRAS, 329, L13
Guainazzi M., Matt G., Fiore F., Perola G. C., 2002, A&A, 388, 787
Harrison F. A. et al., 2013, ApJ, 770, 103
Honma F., Matsumoto R., Kato S., 1991, PASJ, 43, 147
Jansen F. et al., 2001, A&A, 365, L1
Kaspi S., Smith P. S., Netzer H., Maoz D., Jannuzi B. T., Giveon U., 2000, ApJ, 533, 631
Kollatschny W., Fricke K. J., 1985, A&A, 146, L11
Kollatschny W., Bischoff K., Robinson E. L., Welsh W. F., Hill G. J., 2001, A&A, 379, 125
Komossa S., 2015, JHEAp, 7, 148
Komossa S., Bade N., 1999, A&A, 343, 775
Komossa S. et al., 2008, ApJ, 678, L13
Komossa S., Grupe D., Saxton R., Gallo L., 2015, preprint (arXiv:1502.06946)
Korista K. T., Goad M. R., 2004, ApJ, 606, 749
LaMassa S. M. et al., 2015, ApJ, 800, 144
Lamastra A., Bianchi S., Matt G., Perola G. C., Barcons X., Carrera F. J., 2009, A&A, 504, 73
Leighly K. M., Cooper E., Grupe D., Terndrup D. M., Komossa S., 2015, ApJ, 809, L13
MacLeod C. L. et al., 2016, MNRAS, 457, 389
Maiolino R., Marconi A., Salvati M., Risaliti G., Severgnini P., Oliva E., La Franca F., Vanzi L., 2001, A&A, 365, 28
Marchese E., Braito V., Della Ceca R., Caccianiga A., Severgnini P., 2012, MNRAS, 421, 1803
Matt G., Guainazzi M., Maiolino R., 2003, MNRAS, 342, 422
Matt G. et al., 2015, MNRAS, 447, 3029
Miniutti G., Fabian A. C., Brandt W. N., Gallo L. C., Boller T., 2009, MNRAS, 396, L85
Miniutti G., Saxton R. D., Rodríguez-Pascual P. M., Read A. M., Esquej P., Colless M., Dobbie P., Spolaor M., 2013, MNRAS, 433, 1764
Miniutti G. et al., 2014, MNRAS, 437, 1776
Nicastro F., 2000, ApJ, 530, L65
Osterbrock D. E., Ferland G. J., 2006, Astrophysics of Gaseous Nebulae and Active Galactic Nuclei, 2nd edn. University Science Books, Sausalito, CA
Parker M. L. et al., 2014a, MNRAS, 443, 1723
Parker M. L., Schartel N., Komossa S., Grupe D., Santos-Lleó M., Fabian A. C., Mathur S., 2014b, MNRAS, 445, 1039
Penston M. V., Perez E., 1984, MNRAS, 211, 33
Peterson B. M. et al., 1994, ApJ, 425, 622
Pozo Nuñez F. et al., 2015, A&A, 576, A73
Predehl P., Schmitt J. H. M. M., 1995, A&A, 293
Rees M. J., 1988, Nature, 333, 523
Rees M. J., 1990, Science, 247, 817
Reeves J., Done C., Pounds K., Terashima Y., Hayashida K., Anabuki N., Uchino M., Turner M., 2008, MNRAS, 385, L108
Reimers D., Koehler T., Wisotzki L., 1996, A&AS, 115, 235
Ricci C. et al., 2016, ApJ, 820, 5
Risaliti G., Elvis M., Fabbiano G., Baldi A., Zezas A., 2005, ApJ, 623, L93
Ruan J. J. et al., 2015, preprint (arXiv:1509.03634)
Runco J. N. et al., 2016, ApJ, 821, 33
Runnoe J. C. et al., 2016, MNRAS, 455, 1691
Sakata Y. et al., 2010, ApJ, 711, 461
Saxton R. D. et al., 2014, A&A, 572, A1
Schartel N., Rodríguez-Pascual P. M., Santos-Lleó M., Ballo L., Clavel J., Guainazzi M., Jiménez-Bailón E., Piconcelli E., 2007, A&A, 474, 431
Schartel N., Rodríguez-Pascual P. M., Santos-Lleó M., Jiménez-Bailón E., Ballo L., Piconcelli E., 2010, A&A, 512, A75
Schlafly E. F., Finkbeiner D. P., 2011, ApJ, 737, 103
Schlegel D. J., Finkbeiner D. P., Davis M., 1998, ApJ, 500, 525
Shappee B. J. et al., 2014, ApJ, 788, 48
Storchi-Bergmann T., Baldwin J. A., Wilson A. S., 1993, ApJ, 410, L11
Strüder L. et al., 2001, A&A, 365, L18
Titarchuk L., 1994, ApJ, 434, 570
Tohline J. E., Osterbrock D. E., 1976, ApJ, 210, L117
Tombesi F., Cappi M., Reeves J. N., Palumbo G. G. C., Yaqoob T., Braito V., Dadina M., 2010, A&A, 521, A57
Tran H. D., Osterbrock D. E., Martel A., 1992, AJ, 104, 2072
Turner M. J. L. et al., 2001, A&A, 365, L27
Vasudevan R. V., Mushotzky R. F., Winter L. M., Fabian A. C., 2009, MNRAS, 399, 1553
Vestergaard M., Peterson B. M., 2006, ApJ, 641, 689
Voges W. et al., 2000, IAU Circ., 7432, 3
Wang T.-G., Zhou H.-Y., Wang L.-F., Lu H.-L., Xu D., 2011, ApJ, 740, 85
Willingale R., Starling R. L. C., Beardmore A. P., Tanvir N. R., O'Brien P. T., 2013, MNRAS, 431, 394
Wilms J., Allen A., McCray R., 2000, ApJ, 542, 914
Winkler H., Glass I. S., van Wyk F., Marang F., Jones J. H. S., Buckley D. A. H., Sekiguchi K., 1992, MNRAS, 257, 659
Zoghbi A. et al., 2015, ApJ, 799, L24

This paper has been typeset from a TEX/LATEX file prepared by the author.